CAMBRIDGE
UNIVERSITY PRESS

Article

Bosoite, a new silica clathrate mineral from Chiba Prefecture, Japan

Koichi Momma[1]* , Takuji Ikeda[2], Toshiro Nagase[3], Takahiro Kuribayashi[4], Chibune Honma[5], Katsumi Nishikubo[6], Naoki Takahashi[7], Masayuki Takada[8], Yoshitaka Matsushita[9], Ritsuro Miyawaki[1] and Satoshi Matsubara[1]

[1]National Museum of Nature and Science, 4-1-1 Amakubo, Tsukuba, Ibaraki 305-0005, Japan; [2]National Institute of Advanced Industrial Science and Technology (AIST Tohoku), 4-2-1 Nigatake, Miyagino-ku, Sendai 983-8551, Japan; [3]Tohoku University Museum, Aoba, Sendai 980-8578, Japan; [4]Tohoku University, Aoba, Sendai 980-8578, Japan; [5]2345 Kamisanagura, Tateyama, Chiba 294-0038, Japan; [6]593-3, Noda, Iruma, Saitama 358-0054, Japan; [7]Natural History Museum and Institute, Chiba, 955-2 Aoba-cho, Chuo-ku, Chiba 260-8682, Japan; [8]Takada Crystal Museum, 456 Haikata, Oharano, Nishikyo-ku, Kyoto 610-1132, Japan; and [9]National Institute for Materials Science, 1-2-1 Sengen, Tsukuba, Ibaraki 305-0047, Japan

Abstract

Bosoite (IMA2014-023) is a new silica clathrate mineral containing hydrocarbon molecules in its crystal structure. Bosoite can be considered structurally as a silica analogue of the structure-H gas hydrate, where guest molecules are trapped in cage-like voids constructed of the host framework. The mineral occurs in the Miocene tuffaceous sedimentary rocks at Arakawa, Minami-boso City, Chiba Prefecture, Japan. Bosoite is hexagonal, and it crystallises as an epitaxial intergrowth on chibaite crystals, with the {0001} of bosoite parallel to octahedral {111} form of chibaite. Crystals are colourless and transparent with vitreous lustre. The calculated density is 2.04 g/cm^3. The empirical formula (based on 2 O apfu and guest molecules assumed as CH_4) is $Na_{0.01}(Si_{0.98}Al_{0.02})_{\Sigma 1.00}O_2 \cdot 0.50CH_4$; the end-member formula is $SiO_2 \cdot nC_xH_{2x+2}$. Bosoite has the space group $P6/mmm$, with the unit-cell parameters $a = 13.9020(3)$ Å, $c = 11.2802(2)$ Å, $V = 1887.99(6)$ Å^3 and $Z = 34$. The crystal structure of bosoite was refined by single-crystal X-ray diffraction and converged to $R_1 = 4.26\%$ for the average model and $R_1 = 2.96\%$ for the model where all oxygen sites are split.

Introduction

Silica clathrates (or clathrasils) are zeolite-like materials constructed of pure silica framework structures with small cage-like voids. Melanophlogite, a rare silica mineral first reported from Sicily, Italy in the 19th century (von Lasaulx, 1876), is the first example of a silica clathrate. Melanophlogite's chemical composition was at first considered to be essentially SiO_2, and the >6 wt.% C, H and S detected by chemical analyses were thought to be impurities of organic matter trapped as inclusions (Skinner and Appleman, 1963). It turned out to have a crystal structure similar to the cubic structure-I gas hydrate that can incorporate organic molecules (Kamb, 1965). Gas molecules such as CH_4, CO_2, N_2 and H_2S have been reported in natural melanophlogite and noble gases as well as other small molecules can be incorporated into the cages (Gies et al., 1982; Yagi et al., 2007; Tribaudino et al., 2008). Starting from the 1980s, a variety of silica clathrates such as melanophlogite, dodecasil-3C and dodecasil-1H, as well as pure silica zeolites (zeosils) have been synthesised successfully and studied (e.g. Gies et al., 1982; Gies 1984, Gerke and Gies, 1984). For each unique

framework topology, the framework type code (FTC) consisting of three capital letters (in bold type) are assigned by the Structure Commission of the International Zeolite Association (IZA-SC) (Baerlocher et al., 2007). The FTC of melanophlogite is **MEP**.

Chibaite from the Chiba Prefecture, Japan was the second silica clathrate found in Nature (Momma et al., 2011). It has the **MTN**-type framework structure and it is isostructural with the cubic structure-II hydrate. Associated with chibaite, another silica clathrate mineral that is isostructural with the hexagonal structure-H gas hydrate (Lu et al., 2007) was also found. This mineral has been fully characterised and named as bosoite (Momma et al., 2014). Bosoite is the natural analogue of a synthetic silica clathrate compound with the **DOH**-type framework structure, known as dodecasil-1H (Gerke and Gies, 1984). The mineral and its name were approved by the International Mineralogical Association (IMA) Commission on New Minerals, Nomenclature and Classification (IMA2014-023). The mineral is named after the Boso Peninsula, the large peninsula just east of Tokyo across the Tokyo Bay. Type material has been deposited in the collections of the National Museum of Nature and Science, Japan, registered number NMS-M43775 and the Tohoku University Museum, Aoba, Sendai, Japan, mineral collection specimen A-153. A single-crystal X-ray diffraction study was done for both the holotype and cotype (NMS-M43763) samples, and data of the cotype are reported here.

Occurrence

Bosoite occurs in association with chibaite, which was found from Arakawa, Minami-boso City, Chiba Prefecture, Japan (Momma *et al.*, 2011). The Boso Peninsula encompasses the entire Chiba Prefecture located in the middle of the Honshu Island, and Arakawa is located in the south of the Peninsula. Bosoite and chibaite occur in small quartz and calcite veins partly developed at fault planes in tuffaceous sandstone and mudstone of the Miocene Hota Group. They are considered to be a series of forearc sediments deposited near the plate margin by the Palaeo–Izu arc and accreted along the proto-Sagami trough by subduction of the Philippine Sea plate during the Early to Middle Miocene (Ogawa and Ishimaru, 1991; Takahashi *et al.*, 2016).

The sequence of mineral formation from rim to centre of the vein is generally as follows: a very thin layer of clinoptilolite-(Na) and/or opal-A, melanophlogite, chibaite, bosoite and calcite. Melanophlogite 'crystals' were always found as cubic forms of semi-translucent quartz pseudomorphs, with only one exception of an unaltered sample. Many of chibaite 'crystals' are also altered and occur as white quartz pseudomorphs. Some parts of the veins are composed of primary quartz grains or microcrystalline chalcedony. Other associated minerals are pyrite, dachiardite, sepiolite, gypsum and baryte. These minerals were identified by a Gandolfi XRD camera and scanning electron microscopy/energy dispersive X-ray spectrometry (SEM/EDS). The mineral was formed under low-temperature hydrothermal conditions during diagenesis.

Physical and optical properties

Bosoite occurs as an epitaxial intergrowth on chibaite, where the {0001} face of hexagonal bosoite is parallel to the octahedral {111} of chibaite (Figs 1 and 2). It exhibits platy shapes parallel to {0001}. The grain size of an individual crystal is ∼0.01 mm to 0.05 mm thick and 0.05 mm to 0.3 mm in diameter. Crystals are transparent and colourless, have a white streak and a vitreous lustre. Crystals are brittle with an irregular fracture. The Mohs hardness is estimated to be 6½–7 by scratching a thin section sample by hard metal needles. It is non-fluorescent under shortwave or longwave ultraviolet radiation (254 and 365 nm). The density could not be measured because of the small grain size. The calculated density is 2.04 g/cm^3 based on the empirical formula $Na_{0.01}(Si_{0.98}Al_{0.02})_{\Sigma1.00}O_2 \cdot 0.50CH_4$. It is optically uniaxial (+). Due to the small amount of sample available the refractive indices could not be determined. Through observation of the Becke line at grain boundaries between bosoite and chibaite under a polarised light microscope equipped with universal stage, the refractive index (n_ω) of bosoite was found to be slightly higher than that of chibaite, which is optically isotropic and $n = 1.470(1)$.

Raman spectroscopy

Raman spectra (Fig. 3) were measured using a JASCO NRS-5100 spectrometer. Spectra were obtained using a 532 nm laser with the 600 grooves/mm grating and a 100× objective lens. A list of Raman shift positions of the hydrocarbon molecules measured in bosoite are given in Table 1 along with those in the free gas state, in chibaite, and in melanophlogite for comparison. The presence of hydrocarbons is shown by bands in the range 2850 to 3050 cm^{-1}. In the C–H stretching bands, existence of CH_4, C_2H_6, and C_3H_8 or even larger molecules were detected.
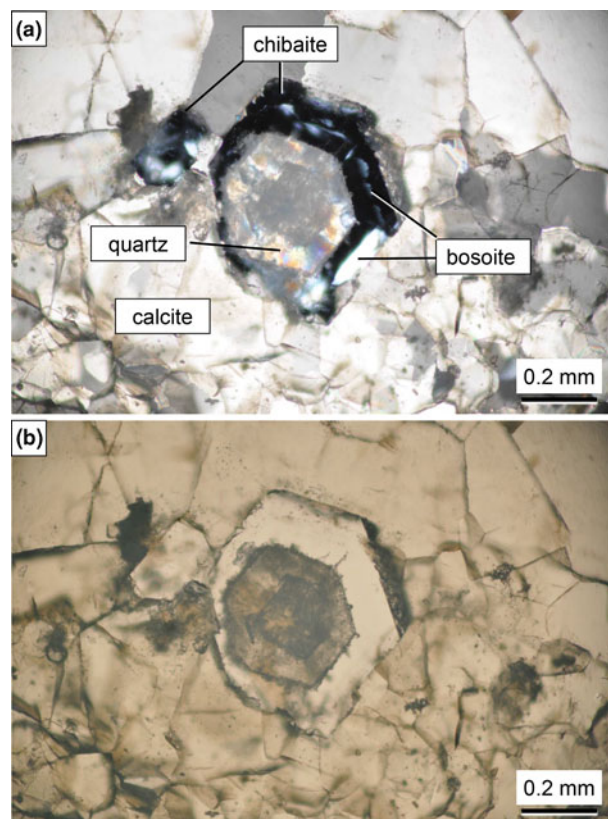

Fig. 1. Photomicrographs of bosoite sample (NSM-M43775) under crossed polarised light (a) and plane polarised light (b). The quartz domain inside chibaite is a pseudomorph of chibaite. The slightly darker area inside the quartz domain is also chibaite overlapped with quartz (see Fig. 2).
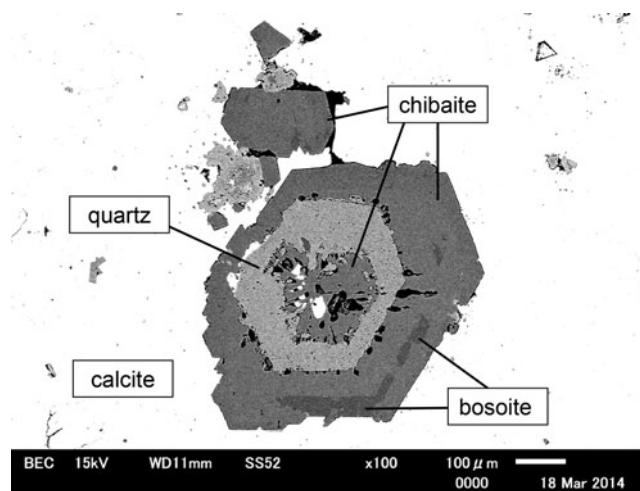
Fig. 2. Back-scattered electron image (BSE) of the sample (NSM-M43775). Bosoite is observed to be slightly darker than chibaite in BSE because the framework density of bosoite (18.0 tetrahedral atoms per 1000 Å^3) is lower than that of chibaite (18.7 tetrahedral atoms per 1000 Å^3).

However, the Raman bands of this region from C_3H_8 or larger molecules do not resolve very well. Signals of C–C stretching bands (∼850–1000 cm^{-1}) could not be detected owing to the high background levels and low signal-to-noise ratios. Therefore, the existence of molecules larger than C_4H_{10} could

Fig. 3. The Raman spectrum of bosoite (NSM-M43775): (a) the whole measured range and (b) enlarged view of the C–H stretching region, overlaid with Raman spectra of chibaite and melanophlogite from the same locality for comparison. Background is subtracted from the data.
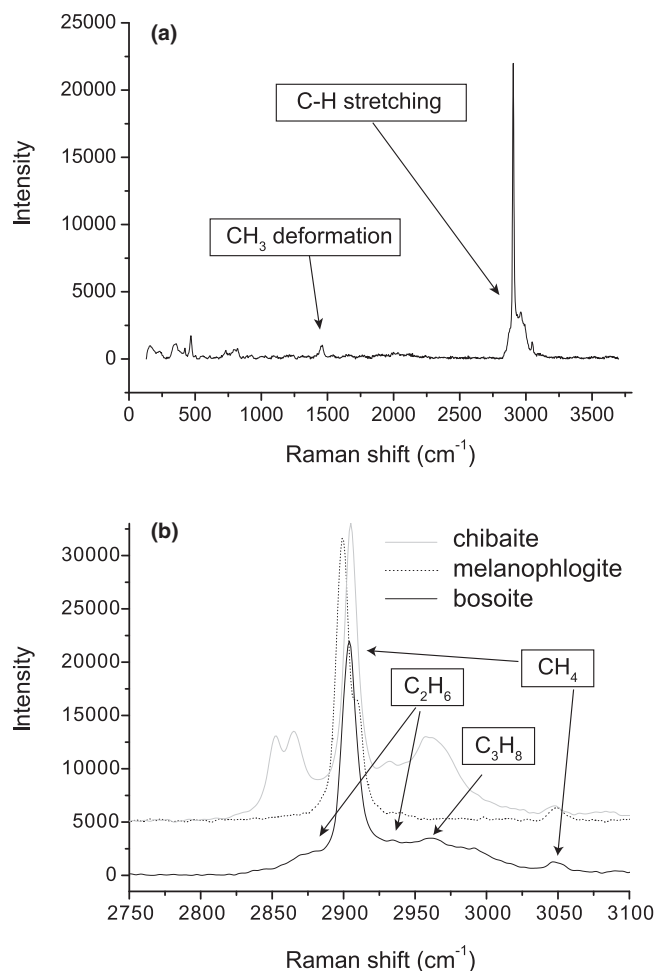
Table 2. Chemical compositions of bosoite.

Constituent	Wt.%	Range	S.D.	Probe standard
SiO_2	86.38	85.10–87.36	0.94	Quartz
Al_2O_3	1.63	1.14–1.96	0.35	Corundum
Na_2O	0.34	0.32–0.37	0.02	Jadeite
$CH_4/C_2H_6/C_3H_8$	11.65*			
Total	100.00			

*Calculated based on the total. S.D. – standard deviation.

$2604 \, cm^{-1}$ (Tribaudino *et al.*, 2008). Raman bands attributable to guest molecules other than hydrocarbons were not observed in bosoite.

Chemical composition

Three quantitative chemical analyses were carried out by means of an electron microprobe (JEOL JXA- 8800M, WDS mode, 15 kV, 5 nA and 1 μm beam diameter). Standard materials for quantitative analyses of the samples were: quartz for Si, corundum for Al and jadeite for Na. The acquired X-ray intensities were corrected by the ZAF method. The analytical results are given in Table 2. Hydrocarbon contents were not measured directly because of the small amounts of material available and thus their quantitative ratios remain undetermined. The total hydrocarbon is given based on the difference and is reported as $CH_4/C_2H_6/C_3H_8$. The empirical formula (based on 2 O atoms per formula unit with an assumption that all the hydrocarbon is CH_4), with rounding errors, is $Na_{0.01}(Si_{0.98}Al_{0.02})_{\Sigma1.00}O_2 \cdot 0.50CH_4$.

A suitable simplified formula is not a straightforward choice since, as noted above, a number of guest molecules could be accommodated in the clathrate. Based on the results of the single-crystal refinement showing a large number of site-scattering factors in the largest cage, the broad Raman bands within the C–H stretching region, and previous studies reporting the necessity of large molecules for crystallisation of the **DOH**-type clathrasil (Gies and Marker, 1992; van Koningsveld and Gies, 2004), hydrocarbon molecules larger than C_4H_{10} are very likely to be included. Assuming just the presence of alkanes in the mineral, the simplified formula is $SiO_2 \cdot nC_xH_{2x+2}$, where x denotes average degree of polymerisation for alkanes and the limit of $(n \times x) \leq {\sim}0.5$. More details about guest molecules are discussed in the Crystallography section below. The stoichiometry $SiO_2 \cdot 0.5CH_4$ requires SiO_2 88.22, CH_4 11.78, total 100.00 wt.%.

not be confirmed. A small peak observed at $1456 \, cm^{-1}$ corresponds to the CH_3 degenerate-deformation modes of alkanes with > 2 C atoms. Raman bands of other possible guest molecules, which have been reported in melanophlogite and chibaite, are as follows. N_2: $2321 \, cm^{-1}$; CO_2: 1277 and 1378 (Kolesov and Geiger, 2003) or $1380 \, cm^{-1}$ (Kanzaki, 2019); H_2S: 2594 and

Table 1. Raman band positions of hydrocarbons in bosoite.

υ_{obs} (cm^{-1})	$\upsilon_{gas/liquid/solid}$ (cm^{-1})	$\upsilon_{(Melanophlogite)}$ (cm^{-1})	$\upsilon_{(chibaite)}$ (cm^{-1})	Assignment Molecule	Vibrational mode
1456	1468.1[e]			Ethane	CH_3 degenerate deformation
	1451[e]			Propane	
	1460[e]			n–Butane	
2870	2900.4[c]		2885[d]	Ethane	C–H region Fermi resonance doublet bands
2904	2917.6[b]	2900[a]	2903[d]	Methane	υ_1 C–H symmetric stretching
		2909[a]	2911[d]		
2935	2955.6[c]		2939[d]	Ethane	
2961	2968.7[e]		2960[f]	Ethane	C–H$_3$ degenerate stretching
	2967[e]			Propane	
	2965[e]			n-Butane	
2992				unassigned	
3049		3047[a]	3051[d]	Methane	$2\upsilon_2$ overtone

[a]Kolesov and Geiger (2003), [b]Sum et al. (1997), [c]Subramanian et al. (2000), [d]Momma et al. (2011), [e]Shimanouchi (1972), [f]Likhacheva et al. (2016).
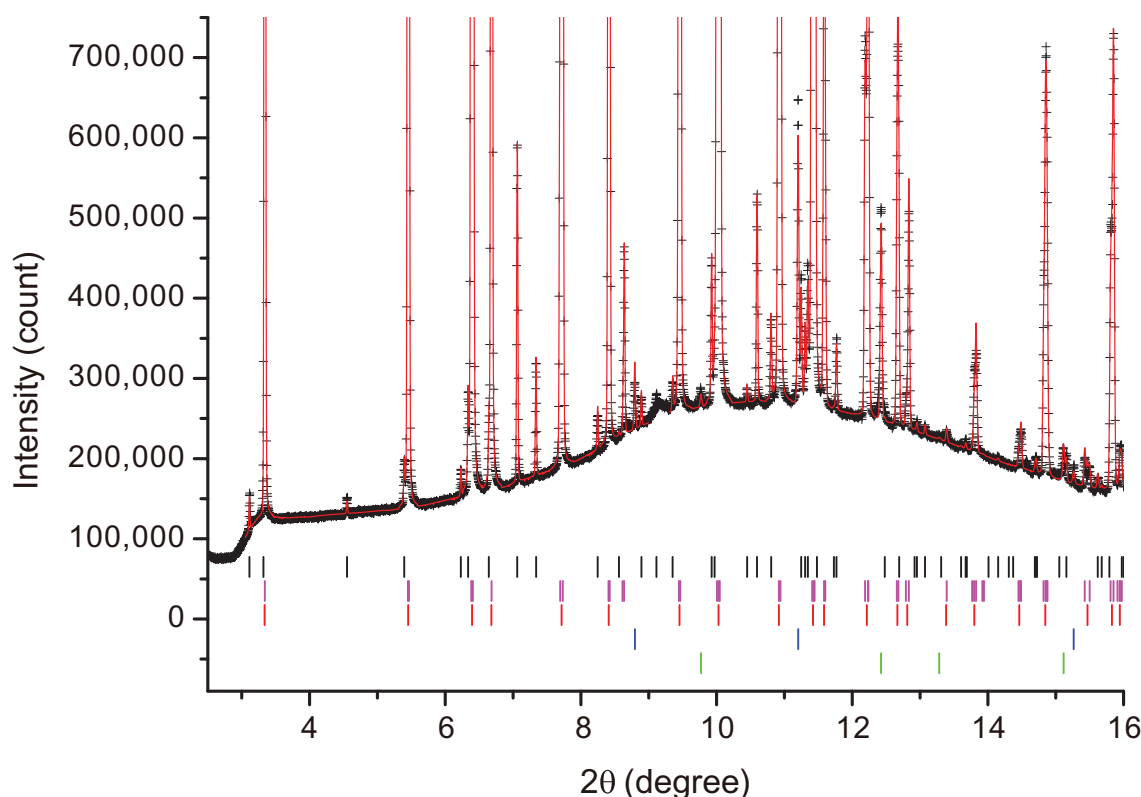
Fig. 4. Observed (black cross) and calculated (solid red line) powder diffraction pattern of sample (NSM-M43775). Tick marks below the pattern indicate diffraction position of bosoite (black), tetragonal phase of chibaite (magenta), cubic phase of chibaite (red), quartz (blue) and calcite (green). Data points from 9.0 to 9.3° were not used in the refinement because a broad halo from opal-A appearing at this range overlaps with a small bosoite peak. When this data range was used, the halo caused significant overestimate of I_o of the overlapped bosoite peak, leading to drifts of various parameters of bosoite.

Crystallography

Powder X-ray diffraction (PXRD) data of the holotype sample were collected by the Debye-Scherrer method with synchrotron radiation using an imaging plate at BL15XU, SPring-8, Japan. As bosoite is always associated with chibaite, the chibaite crystals were separated carefully from the host rock and crushed in an alumina mortar. The obtained powder was sealed in a Lindemann glass capillary tube with inner diameter of 0.5mm. Experimental conditions were as follows: $\lambda = 0.652973$ Å; exposure time = 6 s; and step interval = 0.003°. Data from 3.05° to 56° were used for refinement of unit cell parameters by Rietveld analysis using RIETAN-FP (Izumi and Momma, 2007). Atomic coordinates of bosoite were fixed at values reported by Gerke and Gies (1984) and only occupancies of guest sites and isotropic atomic displacement parameters were refined. For chibaite, both the cubic and tetragonal structural models were used because the symmetry of part of chibaite crystals is low (Momma *et al.*, 2011). Although fitting by two structural models for almost perfectly overlapping peaks might have caused overfitting of chibaite parameters, it was still preferable to retrieve better unit-cell parameters of bosoite. The refinement converged to $R_{wp} = 3.41\%$, $R_p = 2.31\%$, Gof = 15.17, R_{Bragg}(bosoite) = 4.44%, R_F(bosoite) = 2.09%. Note that the high Gof value is due to extremely high signal / background ratio of data. The refined unit-cell parameters of bosoite are $a = 13.8725(3)$, $c = 11.2694(3)$ Å and $V = 1878.18(8)$ Å^3. The refined fraction of each phase is as follows: 2.7 wt.% bosoite; 19 wt.% cubic chibaite; 76 wt.% tetragonal chibaite; 0.9 wt.% quartz; and 1.4 wt.% calcite. Almost all PXRD data of chibaite samples showed the

existence of ~2–3 wt.% of bosoite. Diffraction data are shown in Fig. 4 and listed in Table 3.

Single-crystal X-ray diffraction (SXRD) studies were carried out using a Rigaku R-Axis Rapid II microdiffractometer with Cu$K\alpha$ radiation from the VariMax rotating-anode target combined with a confocal mirror. The epitaxial relation of bosoite and chibaite was confirmed from the holotype sample. However, due to overlap of diffraction peaks of chibaite and bosoite, even small volumes of chibaite associated with bosoite prevented us from doing the structure refinement of bosoite. As the two minerals cannot be distinguished under normal stereomicroscope, we had to make several thin sections to find and cut out a single-crystal of bosoite under polarised light. We decided not to consume the holotype for this purpose and used the cotype because the holotype is much better as a specimen but smaller than the cotype. The Rigaku RAPID AUTO software package (Rigaku, 1998) was used for processing the diffraction data, including the application of numerical absorption correction. The structure was solved by the charge flipping method using *Superflip* (Palatinus and Chapuis, 2007). From the electron-density distributions obtained by the charge flipping method, space group *P6/mmm* reported by Gerke and Gies (1984) was confirmed. All the framework atoms and two guest sites in the small cages were found by the charge flipping method. The rest of the guest sites were found by difference-Fourier syntheses. For the refinement of crystal structure, *SHELXL-2018/1* software (Sheldrick, 2008, 2015) was used, with neutral atom-scattering factors. Details of the data

Table 3. Powder X-ray data (*d* in Å, *I* in %) with normalised intensity of bosoite.

I_{obs}	I_{calc}	d_{obs}	d_{calc}	hkl	I_{obs}	I_{calc}	d_{obs}	d_{calc}	hkl	I_{obs}	I_{calc}	d_{obs}	d_{calc}	hkl
11	8.9	12.002	12.014	100	21	22.9	3.184	3.185	203	3	2.8	1.964	1.964	305
*	2.2	11.198	11.270	001	*	1.3		3.004	400	*	9.8		1.943	423
5	3.4	8.215	8.219	101	4	3.3	2.894	2.894	213	5	7.0	1.887	1.887	602
14*	11.0	6.933	6.936	110	3	3.6	2.868	2.868	312	*	2.8		1.878	006
8	8.3	6.009	6.007	200	3	2.2	2.743	2.743	104	*	1.2		1.867	315
30	23.2	5.907	5.907	111	1.3	1.0	2.652	2.650	402	*	1.1		1.864	432
*	14.6	5.636	5.635	002		1.9		2.553	411	3	4.3	1.832	1.832	610
100	**100.0**	**5.301**	**5.301**	**201**	5	4.5	2.551	2.551	204	*	1.2		1.808	611
33	35.1	5.100	5.102	102	8	9.0	2.475	2.476	322	*	3.2		1.803	405
10	12.9	4.541	4.541	210	3	5.9	2.403	2.403	500	2	2.3	1.787	1.787	334
1.3	1.5	4.374	4.374	112	0.9	1.4	2.394	2.394	214	*	3.0		1.768	424
9	11.0	4.213	4.212	211	*	2.7, 1.5	2.350	2.350, 2.346	501, 403	*	4.2		1.748	433
4	5.7	4.108	4.110	202	4	4.8	2.311	2.312	330	*	2.0		1.745	325
9	10.4	4.006	4.005	300	9	7.2	2.304	2.304	304	3	3.7	1.736	1.736	216
44	**44.2**	**3.773**	**3.774**	**301**	*	3.7		2.222	323	*	1.0		1.714	441
*	7.5		3.757	003	1.7	1.5	2.210	2.210	502		2.3		1.701	306
4	5.6	3.586	3.585	103	1.4	0.6	2.186	2.187	224	*	7.4		1.697	701
62	**68.4**	**3.535**	**3.536**	**212**	1.7	1.1	2.143	2.144	115	*	1.2		1.648	621
24	27.8	3.467	3.468	220	1.0	0.5	2.106	2.106	422	*	2.1		1.644	505
38	**37.4**	**3.331**	**3.332**	**310**	1.2	0.9	2.055	2.055	404	*	1.9		1.632	604
22	23.6	3.315	3.315	221	*	2.3		1.975	430	*	2.2		1.614	335
42*	**33.6**	**3.303**	**3.303**	**113**	2	1.2, 1.3, 1.8	1.969	1.971, 1.970, 1.969	601, 324, 333					
	1.0		3.195	311										

Theoretical powder data are calculated on the basis of the structural model refined by Rietveld analysis using *RIETAN-FP*. For unobserved or overlapped peaks, only calculated lines with *I* > 1 are shown. The strongest lines are given in bold.
*These diffraction peaks were overlapped with peaks of other minerals in the powder sample, i.e. chibaite, quartz and calcite.

Table 4. Data collection and details of the single-crystal structural refinement.

Crystal data		
Structural formula	$SiO_2 \cdot 0.50 CH_4$	
Space group	$P6/mmm$ (#191)	
Unit-cell dimensions	$a = 13.9020(3)$, $c = 11.2802(2)$	
Volume (Å^3)	$V = 1887.99(6)$	
Z	34	
D_{calc} (g/cm^3)	2.04	
F000	1190	
μ (mm^{-1})	6.5	
Crystal size (mm)	0.060 × 0.050 × 0.040	
Data collection		
Temperature (K)	293(2)	
Radiation	Cu$K\alpha$ ($\lambda = 1.54187$ Å)	
Voltage, current	40 kV, 30 mA	
$2\theta_{max}$ (°)	136.4	
No. of reflections measured	22,203	
Independent reflections ($I > 2\sigma(I)$)	739 (705, $R_{int} = 0.031$)	
Indices range of *h, k, l*	$-16 \leq h \leq 16$, $-16 \leq k \leq 16$, $-13 \leq l \leq 13$,	
Absorption correction	Numerical (*NUMABS*; Higashi, 1999)	
Max. and min. transmission factors	0.710–0.771	
Refinement	Average model	Disordered model
No. of variables / restraints	73 / 0	138 / 15
Reflection/Parameter Ratio	10.1	5.36
R_1, wR_2 ($I > 2\sigma(I)$)	0.043, 0.120	0.030, 0.085
R_1, wR_2 (All reflections)	0.044, 0.121	0.030, 0.086
Goodness-of-fit:	1.17	1.09
$\Delta\rho_{max}$, $\Delta\rho_{min}$ (e^-/Å^3)	0.55 and −0.34	0.43 and −0.27

collection, refinement, and results of the refinement are summarised in Table 4.

An illustration of the average crystal structure is shown in Fig. 5. Refined atomic coordinates and equivalent isotropic displacement parameters are summarised in Table 5. Selected bond distances and bond angles are given in Table 6. From the difference-Fourier map, all of oxygen atom positions were found to be split around their average positions. Subsequent refinements with all the O sites split around their average positions greatly reduced the residual electron densities and improved *R*1 from 4.26% to 2.96% with a trade-off of poorer data / parameter ratio. The mean U_{eq} of O sites also changed from 0.076 Å^2 to 0.039 Å^2. To reduce the number of free parameters and their correlations, occupancy of each split O site was fixed at ⅓ and the position of each O site was restrained such that it is placed equidistant from neighbouring Si sites. Anisotropic displacement components of the split O atoms along the adjacent O–O direction were also restrained to be equal by using the *DELU* instruction. The crystallographic information files containing results of the refinements based on the average and split models have been deposited with the Principal Editor of *Mineralogical Magazine* and are available as Supplementary material (see below).

The unit cell of bosoite consists of three types of cages: two $[4^3 5^6 6^3]$ cages, three $[5^{12}]$ cages and one $[5^{12} 6^8]$ cage (here $[4^i 5^j 6^k]$ denotes a polyhedron having *i* quadrilateral, *j* pentagonal and *k* hexagonal faces). The former two types of cages are relatively small and mainly occupied by CH_4. C1 and C2 atoms are those of CH_4 molecules at the centre of $[4^3 5^6 6^3]$ and $[5^{12}]$ cages respectively, and their U_{eq} are relatively large owing to very weak van der Waals interaction with the host framework. Occupancies of these sites were fixed at 1 because they exceeded 1 when freely refined. Furthermore, the difference-Fourier map still showed small residuals around C1 and C2 atoms. Distances from C1 and C2 atoms to the residuals were ~1 Å and these residuals were interpreted as orientationally disordered hydrogen atoms of CH_4. When these H atoms were included in the refinement with their U_{iso} values constrained to the same and C–H distances fixed to 1.08 Å, R indices decreased ~0.3%. In the final refinement of the average model, these H atoms are not included because they are less reliable, whereas they are included in the split model for reference. In the largest $[5^{12} 6^8]$ cage, large
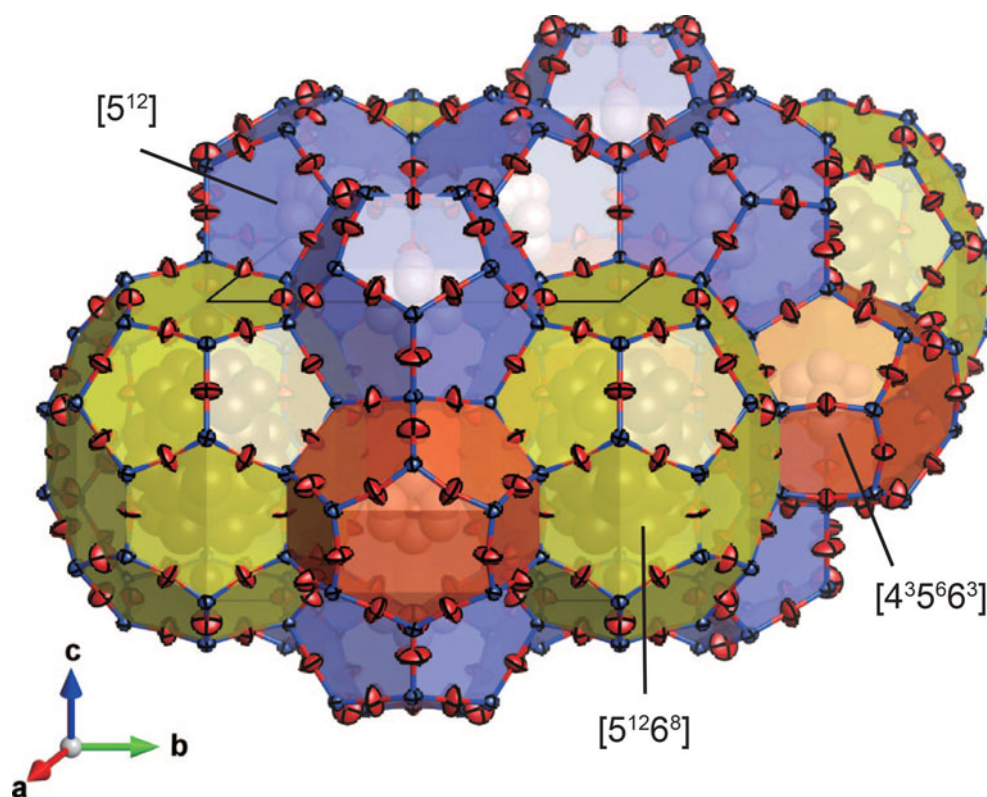
Fig. 5. The average framework structure of bosoite refined without splitting of O sites.

Table 5. Refined atomic position and equivalent isotropic displacement parameters (Å²) of the average model.

	Wyk.	x	y	z	U_{eq}/U_{iso}	Occ.
Si1	12o	0.41870(9)	0.20935(4)	0.22527(9)	0.0300(4)	1
Si2	12n	0.38736(8)	0.38736(8)	0.36254(9)	0.0305(4)	1
Si3	6l	0.26279(12)	0.13140(6)	0	0.0296(4)	1
Si4	4h	⅔	⅓	0.13850(15)	0.0318(5)	1
O1	24r	0.3946(3)	0.2885(2)	0.3036(3)	0.0786(10)	1
O2	12o	0.5438(3)	0.27189(15)	0.1844(4)	0.0836(14)	1
O3	12o	0.3394(3)	0.16968(17)	0.1142(3)	0.0724(12)	1
O4	6k	0.3616(4)	0	½	0.0611(15)	1
O5	6j	0.1850(4)	0	0	0.0651(15)	1
O6	6i	½	0	0.3425(5)	0.0725(18)	1
O7	2c	⅔	⅓	0	0.102(4)	1
C1	2d	⅓	⅔	½	0.127(9)	1
C2	3f	½	0	0	0.137(8)	1
C3A	2e	0	0	0.265(9)	0.28(7)*	0.73(14)
C3B	12o	−0.044(3)	0.044(3)	0.571(6)	0.28*	0.30(3)
C3C	12n	0	0.112(6)	0.315(6)	0.28*	0.33(3)
C3D	2e	0	0	0.06(2)	0.28*	0.21(6)
C3E	6m	0.177(8)	0.088(4)	½	0.28*	0.50(6)

*U_{iso} were refined with their values constrained to the same.

Table 6. Selected bond distances and bond angles in bosoite.

	Distance (Å)		Angle(°)
Si1–O1 ×2	1.573(2)	Si1–O1–Si2	167.7(2)
Si1–O2	1.575(4)	Si4–O2–Si1	177.7(4)
Si1–O3	1.575(3)	Si1–O3–Si3	178.3(3)
Si2–O1 ×2	1.574(2)	Si2–O4–Si2	154.0(4)
Si2–O6	1.5821(13)	Si3–O5–Si3	167.8(4)
Si2–O4	1.5914(15)	Si2–O6–Si2	163.6(4)
Si3–O3 ×2	1.584(3)	Si4–O7–Si4	180
Si3–O5 ×2	1.5909(10)		
Si4–O7	1.5623(17)		
Si4–O2 ×3	1.568(4)		
<Si–O>	1.578	<Si–O–Si>	170

number of guest C atoms in the unit cell is ∼13.1–14.5. Assuming that widely spread electrons of H atoms in the [$5^{12}6^8$] cage were not fully reflected to the refined site-scattering factor, and the [$5^{12}6^8$] cage is occupied mainly by large hydrocarbons, these numbers are within an acceptable range compared to the number estimated by the chemical analysis (17C per unit cell).

The electron-density distribution in bosoite calculated by the maximum entropy method (MEM) is shown in Fig. 6. *Dysnomia* (Momma *et al.*, 2013) with the *L-BFGS* algorithm was used for calculation and *VESTA* (Momma and Izumi, 2011) was used for visualisation. To reduce correlation of residuals $|F_o – F_c| / σ(F_o)$ with d spacing of reflections, an exponential-type weighting scheme proportional to $m \times \exp(–A/d)$ was used, where m is multiplicity of reflections and A is a weighting parameter optimised as 12.7. The electron-density distribution also confirms that all cages are almost fully occupied.
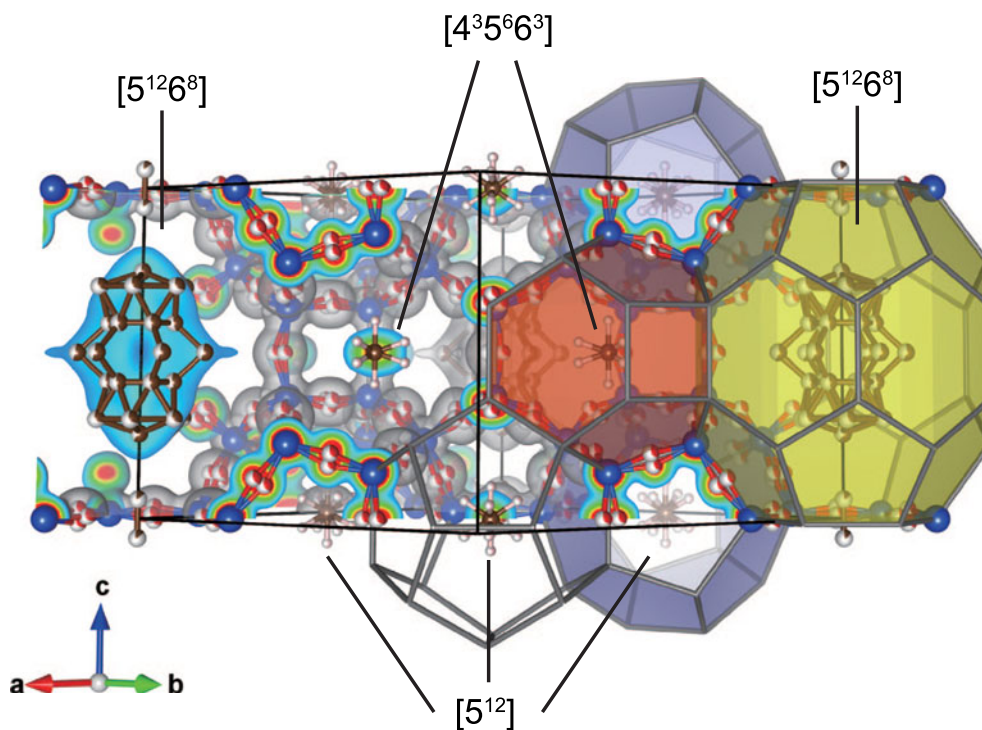
molecules or multiple number of small molecules are included. The total site-scattering factor in the [$5^{12}6^8$] cage, refined as occupancies of C, was 81 e^-. The refined U_{iso} of C3A to C3E in the [$5^{12}6^8$] cage are extremely large owing to the variety of guest species and their static/dynamic disorder. Therefore, guest species and their ratio in the [$5^{12}6^8$] cage could not be interpreted. Depending on average degree of polymerisation for alkanes, 81 e^- corresponds to 8.1 CH_4, 4.5 C_2H_6, 3.12 C_3H_8, or 2.38 C_4H_{10} molecules. When these four cases are considered, the total

Fig. 6. Electron-density distribution in bosoite determined by MEM analysis overlapped with the split atom model. Isosurface level is 0.5 e^-/Å^3.

Discussion

The order of crystallisation of melanophlogite, chibaite and bosoite observed in the present study indicates a decisive role of guest molecules on their crystallisation. The $[5^{12}]$ cage is common to all three minerals. Other types of cages making-up these minerals are: the $[5^{12}6^2]$ cage in melanophlogite, the $[5^{12}6^4]$ cage in chibaite as well as the $[4^35^66^3]$ and the $[5^{12}6^8]$ cages in bosoite. The $[5^{12}6^8]$ cage is the largest and the $[5^{12}]$ cage is the smallest among them, whereas the $[4^35^66^3]$ cage is comparable in size to the smallest $[5^{12}]$ cage. From the previous studies on syntheses of these clathrasils, the presence of large molecules matching in size to the largest cage in the crystal structure is considered as a necessary condition for their crystallisation (e.g. van Koningsveld and Gies, 2004). This model can explain why bosoite was always found associated with chibaite crystals and why it is so minor in volume compared to the other two. The $[5^{12}6^2]$ cage in melanophlogite can incorporate small gas molecules such as CH_4, CO_2, N_2 and H_2S, which are abundant gases in Nature. As a result, among these clathrasils, melanophlogite is the most abundant and the first phase to crystallise in Nature. While C_2H_6 is also capable of fitting into the $[5^{12}6^2]$ cage (Ohno *et al.*, 2009), C_3H_8 or larger hydrocarbons are too large for melanophlogite. As a result, the concentration of these large molecules in hydrothermal solutions increases as melanophlogite crystallises, and eventually crystallisation of chibaite is initiated. Similarly, the increase of the concentration of even larger molecules that cannot fit into the chibaite structure would initiate crystallisation of bosoite. As bosoite grows, large molecules would be consumed easily and overgrowth of chibaite on bosoite also occurs. Larger hydrocarbons have higher molecular refraction. Therefore, the above model of crystallisation is also consistent with the fact that the refractive index of bosoite is higher than that of chibaite regardless that the framework density of bosoite is lower than that of chibaite.

Our observation that melanophlogite was almost always found to be replaced by quartz indicates that melanophlogite is less stable than both chibaite and bosoite.

SiO_4 tetrahedra in framework silicates are known to be very stiff, to a first approximation they behave more like rigid units which rotate and translate without distortion of the tetrahedra (Hammonds *et al.*, 1996). On the other hand, the apparently short Si–O distances are often reported for clathrasils as a consequence of local tilting of the SiO_4 tetrahedra with the rigid-unit mode, where Si–O distances are almost constant but actual O atoms are distributed around the refined positions (Momma, 2014). This is why in the refinement of bosoite without splitting of O sites, the mean value of Si–O distance (1.578 Å) apparently looks shorter than the predicted value, 1.609 Å, for tetrahedrally coordinated pure silica frameworks (Brown *et al.*, 1969; Wragg *et al.*, 2008). Si–O–Si angles range from 154.0(4)° to 180° with a mean value of 170°, which is also larger than the average value of 154° ± 9 for pure silica zeolite frameworks (Wragg *et al.*, 2008). With the splitting of O sites, mean values of Si–O distances and Si–O–Si angles changed to 1.604 Å and 156° respectively. The splitting of O sites due to local disorder has also been reported for synthetic **MTN**- and **DOH**-type clathrasils (Könnecke *et al.*, 1992; Miehe *et al.*, 1993). In the case of melanophlogite and chibaite, the tilting of the framework SiO_4 tetrahedra at ambient or low temperature causes lowering of their space group symmetries (e.g. Nakagawa *et al.*, 2001; Scheidl *et al.*, 2018). On the other hand, as was reported for the synthetic **DOH**-type clathrasil (Miehe *et al.*, 1993), we could see no sign of symmetry lowering of bosoite even though all of the O sites were found to be split.

References

Baerlocher C., McCusker L.B. and Olson D.H. (2007) *Atlas of Zeolite Framework Types*. Elsevier, Amsterdam.

Brown G.E., Gibbs G.V. and Ribbe P.H. (1969) The nature and variation in length of the Si–O and Al–O bonds in framework silicates. *American Mineralogist*, **54**, 1044–1061.

Gerke H. and Gies H. (1984) Studies on clathrasils. IV: Crystal structure of dodecasil 1H, a synthetic clathrate compound of silica. *Zeitschrift für Kristallographie*, **166**, 11–22.

Gies H. (1984) Studies on Clathrasils. VI. Crystal structure of dodecasil 3C, another synthetic clathrate compound of silica. *Zeitschrift für Kristallographie*, **167**, 73–82.

Gies H. and Marker B. (1992) The structure-controlling role of organic templates for the synthesis of porosils in the systems SiO_2/template/H_2O. *Zeolites*, **12**, 42–49.

Gies H., Gerke H. and Liebau F. (1982) Chemical composition and synthesis of melanophlogite, a clathrate compound of silica. *Neues Jahrbuch für Mineralogie, Monatshefte*, **3**, 119–124.

Hammonds K.D., Dove M.T., Giddy A.P., Heine V. and Winkler B. (1996) Rigid-unit phonon modes and structural phase transitions in framework silicates. *American Mineralogist*, **81**, 1057–1079.

Higashi, T. (1999) *NUMABS*. Rigaku Corporation, Tokyo, Japan.

Izumi F. and Momma K. (2007) Three-dimensional visualization in powder diffraction. *Solid State Phenomena*, **130**, 15–20.

Kamb B. (1965) A clathrate crystalline form of silica. *Science*, **148**, 232–234.

Kanzaki M. (2019) High-temperature Raman spectroscopic study of CO_2-containing melanophlogite. *Journal of Mineralogical and Petrological Sciences*, **114**, 122–129.

Kolesov B.A. and Geiger C.A. (2003) Molecules in the SiO_2-clathrate melanophlogite: a single-crystal Raman study. *American Mineralogist*, **88**, 1364–1368.

Könnecke M., Miehe G. and Fuess H. (1992) Static disorder of dodecasil 3C. A single-crystal study with synchrotron radiation. *Zeitschrift für Kristallographie*, **201**, 147–155.

Likhacheva A.Y., Goryainov S.V., Seryotkin Y.V., Litasov K.D. and Momma K. (2016) Raman spectroscopy of chibaite, natural MTN silica clathrate, at high pressure up to 8 GPa. *Microporous and Mesoporous Materials*, **224**, 100–106.

Lu H., Seo Y.-T., Lee J.-W., Moudrakovski I., Ripmeester J. A., Chapman N.R., Coffin R.B., Garder G. and Pohlman J. (2007) Complex gas hydrate from the Cascadia margin. *Nature*, **445**, 303–306.

Miehe G., Vogt T., Fuess H. and Müller, U. (1993) A study of disorder in the SiO_2 host lattice of dodecasil 1H using synchrotron radiation. *Acta Crystallographica*, **B49**, 745–754.

Momma K. (2014) Clathrate compounds of silica. *Journal of Physics: Condensed Matter*, **26**, 103203.

Momma K. and Izumi F. (2011) VESTA 3 for three-dimensional visualization of crystal, volumetric and morphology data. *Journal of Applied Crystallography*, **44**, 1272–1276.

Momma K., Ikeda T., Nishikubo K., Takahashi N., Honma C., Takada M., Furukawa Y., Nagase T. and Kudoh Y. (2011) New silica clathrate minerals that are isostructural with natural gas hydrates. *Nature Communications*, **2**, 196.

Momma K., Ikeda T., Belik A.A. and Izumi, F. (2013) Dysnomia, a computer program for maximum-entropy method (MEM) analysis and its performance in the MEM-based pattern fitting. *Powder Diffraction*, **28**, 184–193.

Momma K., Ikeda T., Nagase T., Kuribayashi T., Honma C., Nishikubo K., Takahashi N., Takada M., Matsushita Y., Miyawaki R. and Matsubara S. (2014) Bosoite, IMA 2014-023. CNMNC Newsletter No. 21, August 2014, page 800; *Mineralogical Magazine*, **78**, 797–804.

Nakagawa T., Kihara K. and Harada K. (2001) The crystal structure of low melanophlogite. *American Mineralogist*, **86**, 1506–1512.

Ogawa Y. and Ishimaru K. (1991) Geological structures of the Emi Group on the coast of the Emi area, southern part of the Boso Peninsula, Central Honshu. *Journal of Geography*, **100**, 530–539 [in Japanese with English abstract].

Ohno H., Strobel T.A., Dec S.F., Sloan E.D. and Koh, C.A. (2009). Raman studies of methane-ethane hydrate metastability. *Journal of Physical Chemistry A*, **113**, 1711–1716.

Palatinus, L. and Chapuis G. (2007) SUPERFLIP– a computer program for the solution of crystal structures by charge flipping in arbitrary dimensions. *Journal of Applied Crystallography*, **40**, 786–790.

Rigaku (1998) *RAPID-AUTO*. Rigaku Corporation, Tokyo, Japan.

Scheidl K.S., Effenberger H.S., Yagi T., Momma K. and Miletich, R. (2018) The hydrocarbon-bearing clathrasil chibaite and its host-guest structure at low temperature. *IUCrJ*, **5**, 595–607.

Sheldrick G.M. (2008) A short history of SHELX. *Acta Crystallographica*, **A64**, 112–122.

Sheldrick G.M. (2015) Crystal structure refinement with SHELXL. *Acta Crystallographica*, **C71**, 3–8.

Shimanouchi T. (1972) *Tables of Molecular Vibrational Frequencies, Consolidated Volume I*. National Bureau of Standards, Gaithersburg, MD, USA.

Skinner B.J. and Appleman, D.E. (1963) Melanophlogite, a cubic polymorph of silica. *American Mineralogist*, **48**, 854–867.

Subramanian S., Kini R.A., Dec S.F. and Sloan E.D. (2000) Evidence of structure II hydrate formation from methane + ethane mixtures. *Chemical Engineering Science*, **55**, 1981–1999.

Sum A.K., Burruss R.B. and Sloan E.D. (1997) Measurement of clathrate hydrates via Raman spectroscopy. *Journal of Physical Chemistry B*, **101**, 7371–7377.

Takahashi N., Shibata K., Hirata D. and Niida S. (2016). Geologic traverse from the Mineoka Belt to the Hayama Belt, Central Japan. *Journal of the Geological Society of Japan*, **122**, 375–395 [in Japanese].

Tribaudino M., Artoni A., Mavris C., Bersani D., Lottici P.P. and Belletti D. (2008) Single-crystal X-ray and Raman investigation on melanophlogite from Varano Marchesi (Parma, Italy). *American Mineralogist*, **93**, 88–94.

van Koningsveld H. and Gies H. (2004) Similarities between the clathrasils DOH, DDR, MEP and MTN. *Zeitschrift für Kristallographie*, **219**, 637–643.

von Lasaulx A. (1876) Mineralogisch-krystallographische Notizen. VII. Melanophlogit, ein neues Mineral. *Neues Jahrbuch für Mineralogie*, 250–257.

Wragg D.S., Morris R.E. and Burton, A.W. (2008) Pure silica zeolite-type frameworks: A structural analysis. *Chemistry of Materials*, **20**, 1561–1570.

Yagi T., Iida E., Hirai H., Miyajima N., Kikegawa T. and Bunno, M. (2007) High-pressure behavior of a SiO_2 clathrate observed by using various pressure media. *Physical Review B*, **75**, 174115.